Synthesis of multifunctional microdiamonds on stainless steel substrates by chemical vapor deposition

Article *in* Carbon · January 2021

DOI: 10.1016/j.carbon.2020.09.064

CITATIONS
10

READS
195

5 authors, including:

Pratik Joshi
North Carolina State University
26 PUBLICATIONS **148** CITATIONS
SEE PROFILE

Ariful Haque
Texas State University
46 PUBLICATIONS **670** CITATIONS
SEE PROFILE

Siddharth Gupta
North Carolina State University
39 PUBLICATIONS **477** CITATIONS
SEE PROFILE

J. Narayan
North Carolina State University
1,085 PUBLICATIONS **31,655** CITATIONS
SEE PROFILE

Carbon 171 (2021) 739–749

Contents lists available at ScienceDirect

Carbon

journal homepage: www.elsevier.com/locate/carbon

Research Article

Synthesis of multifunctional microdiamonds on stainless steel substrates by chemical vapor deposition

Pratik Joshi [a], Ariful Haque [a, b], Siddharth Gupta [a, b], Roger J. Narayan [c], Jagdish Narayan [a, *]

[a] Department of Materials Science and Engineering, North Carolina State University, Raleigh, NC, 27695-7907, USA
[b] Intel Corporation, Rolner Acres Campus 3, OR, 97124, USA
[c] Department of Biomedical Engineering, North Carolina State University, Raleigh, NC, 27695-7907, USA

ARTICLE INFO

Article history:
Received 19 July 2020
Received in revised form
9 September 2020
Accepted 15 September 2020
Available online 28 September 2020

Keywords:
Laser annealing
Q-carbon
Diamond thin films
Stress
EBSD
Raman spectroscopy

ABSTRACT

We report on the synthesis of multifunctional microdiamonds by chemical vapor deposition (CVD) on 304 and 316 austenitic stainless steel (SS) substrates. The increase in wettability achieved by surface scratching and the structure of ultra-dense Q-carbon achieved high nucleation density and minimized strains in diamond films. Notably, these diamond films exhibit a high amount of twinning, leading to the formation of five-fold microdiamonds. The diamonds on scratched SS substrate and Q-carbon interlayer exhibit a full width at half maximum of 8.25 cm^{-1} and 11.5 cm^{-1}, compared to 26 cm^{-1} on bare SS substrate. The diamond films grown on bare SS substrate exhibited cracking due to high tensile stress of 2.3 GPa, ascribed to thermal mismatch between SS and diamond. The electron backscattered diffraction investigations reveal iron inclusions in diamonds synthesized on bare SS substrates, which may create ferromagnetism in these diamonds. This route, compared to the ion beam implantation method using ferromagnetic ions, yields better samples. At 800 °C, 10^{12} Fe atoms/cm^2s are transferred from the SS substrate into the diamonds. The dominant growth orientation for these CVD diamonds was determined to be <110> out of plane. These multifunctional microdiamonds are useful for biomedical, electronic, and tribological applications.

Published by Elsevier Ltd.

1. Introduction

Diamond possesses highly useful properties such as high thermal conductivity, high refractive index, high bandgap, high hardness, and excellent biocompatibility [1,2]. Majority of the diamonds: both natural and artificial are diamagnetic. Future electronic and biomedical applications involving targeted drug delivery to a specific site, magnetic semiconductors for electronic applications (by controlling the quantum state of the electron spin) are possible by utilizing ferromagnetic diamonds [3–5]. Diamonds can be rendered ferromagnetic by incorporating inclusions in them. Magnetic inclusions like iron oxides and sulfides render naturally occurring diamonds magnetic [6]. Iron carbide inclusions can also make diamonds ferromagnetic [7]. Iron carbide (Fe_3C), also known as cementite, crystallizes in the orthorhombic crystal structure; it has ferromagnetic nature with a Curie temperature of approximately 187 °C [8]. There is a consensus that synthetic diamonds fabricated by CVD are diamagnetic if there is no contamination by ferromagnetic impurities. However, recent studies have reported the growth of magnetic CVD diamonds with a saturation magnetization of 0.3 emu/g on stainless steel (SS) foil, suggesting that the magnetic nature of CVD diamonds is highly dependent on the substrate on which they are fabricated. The magnetism of diamonds fabrication on SS foil has been attributed to the presence of iron, chromium, and nickel in diamonds that were picked up from the SS substrate [5,9]. The incorporation of these species from the substrate into diamond is not well understood, making it necessary to perform more studies on the phenomenon of ferromagnetism in CVD diamonds synthesized on austenitic SS substrates. Studies have also been performed to inject Fe ions by using ion implantation in nanodiamonds to make them magnetic [10]. However, the defects generated can only be removed by 2 step high-temperature annealing process which can lead to graphitization. Hence, CVD processing to generate ferromagnetic diamonds compared to ion implantation is convenient from processing point of view.

The phenomenon of diamond film cracking and delamination as a function of the substrate has been studied in great detail. Lattice mismatch strain and thermal mismatch strain are two significant

* Corresponding author.
E-mail address: narayan@ncsu.edu (J. Narayan).

https://doi.org/10.1016/j.carbon.2020.09.064
0008-6223/Published by Elsevier Ltd.

contributors to diamond film cracking. To minimize thermal strain (ε_T) between the diamond film and the substrate, there should be minimal difference in the thermal expansion coefficient (α) between the substrate and the coating as $\varepsilon_T = \Delta\alpha\Delta T$. Previously, it has been observed that the formation of graphite is catalyzed on transition metals which have incompletely filled 3d shells [11]. Ferrous substrates predominantly exhibit diamond thin film delamination due to the formation of interposing graphitic layers at substrate temperatures upto 900 °C [11,12]. Notably, the thermal expansion coefficient (TEC) of steels varies from 9×10^{-6}/°C to 1.8×10^{-5}/°C in comparison with 1.0×10^{-6}/°C for the diamond at 300 K [13]. In the whole steel family, austenitic SS has the highest TEC value resulting in a maximum thermal mismatch between the SS substrate and the deposited diamond coating on it. It causes cracking and delamination of the coating. The thermal stress as a function of thermal strain can be calculated using $\sigma_T = \frac{2\mu(1+\vartheta)}{(1-\vartheta)}\varepsilon_T$. The terms μ and ϑ are shear modulus and Poison's ratio of diamond, respectively. This yields a high value of 6–8 GPa generated in a diamond film on steel substrates [14]. However, biomedical and tribological applications necessitate high-quality diamond coatings on SS. Nevertheless, due to the myriad of issues discussed above, only a limited number of studies have been carried out to investigate diamond deposition on austenitic SS.

Researchers have contemplated various methods to improve the quality of diamond film synthesized on ferrous substrates. The most popular concept has been the use of interlayer, which acts as a barrier for diffusion, preventing the reaction between the substrate and the gases used to synthesize diamond during CVD. It can, in some cases, assist in reducing the TEC mismatch. Interestingly, the interlayer may also promote diamond nucleation by providing diamond nucleation sites, if the interlayer is a carbide former with an atomic structure similar to the diamond cubic. The metastable allotrope of carbon (Q-carbon), which has a higher mass density than diamond, can provide diamond nucleation sites as well as minimize thermal stress, because of similar TEC as that of diamond. The Q-carbon forms when liquid carbon is quenched at rates exceeding 10^9 K/s [15,16], Q-carbon interlayer has shown promising results to obtain a continuous diamond film on metallic [17], and sapphire [18–20] substrates. The formation of Q-carbon at 4000 K results in nano-welded regions with the substrate giving rise to superior adhesion between the film and the substrate [21]. In the case of sapphire, it has been surmised that the liquid carbon can react with Al_2O_3 and form Al_4C_3, making it possible to synthesize diamond film with improved adhesion and containing a higher number density of diamonds [22]. Previously, pulsed laser annealing (PLA) substrate prior to CVD has been shown to be effective in producing high-quality diamonds at lower CVD substrate temperatures than usually necessary [14,23]. Furthermore, additional adhesion improvement is possible by diamond seeding the substrate followed by PLA to melt the substrate to embed the diamond seeds into the substrate [24–26].

The purpose of this study is two-fold, first to shed light on the formation of possibly ferromagnetic CVD diamonds on paramagnetic austenitic 304 SS and 316 SS, and second, to compare the effectiveness of surface scratching and Q-carbon interlayer in producing high-quality CVD diamonds on austenitic SS. Scratching is a common method to increase diamond nucleation [27]. However, the novelty aspect of this work is to compare the quality of CVD grown diamond on surface scratch and Q-carbon interlayer. The surface morphologies and structure of these diamonds have been investigated systematically. The inclusions responsible for inducing ferromagnetism in CVD diamonds have been characterized, and their formation rationalized using Gibbs free energy analysis. We have quantified the difference in the quality and residual stresses in the diamond film on austenitic SS due to the presence of surface scratches and the Q-carbon interlayer using Raman spectroscopy, electron backscattered diffraction (EBSD), high-resolution scanning electron microscopy (HRSEM), and x-ray diffraction (XRD).

2. Experimental methods

2.1. Hot filament chemical vapor deposition (HFCVD)

HFCVD was carried out at a substrate temperature of 775±25 °C for a growth duration of 3 and 6 h in a steel chamber with a water-cooling facility. Four filaments of tungsten with a diameter of 508 μm each were utilized. A voltage of 9±0.1 V was applied across the filaments, and a current of 90±10 A was passed through the filament(s). This resulted in the tungsten filaments getting heated to a high-temperature of ~2000 °C. The distance between the filament and the substrate was measured using Vernier caliper and maintained at ~4–6 mm. The Carburization process was carried out before the beginning of the growth process for ~30 min at a flow rate of 50 sccm (standard cubic centimeter per minute) for CH_4 and 10 sccm for H_2 gas at a chamber pressure of 10 Torr. The CVD growth was carried under a flow rate of 2 sccm for CH_4 and 100 sccm for H_2 at a chamber pressure of 20 Torr. The gas flow rates were measured using mass flow controllers (MKS Instruments, Inc). The samples were placed on a heat resistant Molybdenum heater block. The filament temperature was measured with a two-color pyrometer, and the substrate temperature was measured by a contactless optical pyrometer through a glass lens present in the chamber. After the deposition, substrate was cooled at a constant cooling rate of 10 °C/min to minimize the thermal shock effect.

2.2. Substrate pretreatment, cleaning procedure, and seeding process

Austenitic SS substrates 304 and 316 were polished using Kempad lapping disc manufactured by Allied High Tech Products. The disc was sprayed with diamond in water colloidal suspension in order of 9 μm, 6 μm, 3 μm, and 1 μm grade. After polishing at each grade, the samples were washed with deionized water and cleaned with acetone and methanol before switching to a finer grade on a new lapping disc. All the polished samples (SS 304, 316, Silicon, sapphire) were cleaned using acetone and methanol in an ultrasonic cleaning bath for 5 min each at room temperature. The samples were handled with nonmagnetic tweezers manufactured by DuPont. The stainless-steel substrate surface was scratched by utilizing a diamond scriber. Before performing CVD, all the samples were cleaned with a high velocity N_2 gas jet. For just seeding purposes, 50 nm diamond in colloidal water suspension was sprayed on the samples.

2.3. Formation of Q-carbon interlayer

The technique of pulsed laser deposition (PLD) was used to coat austenitic SS 304/316 with a 200–400 nm thick diamond-like carbon (DLC) layer corresponding to 2000 laser shots on Ti-doped glassy carbon target. The optimum amount of Ti doping was utilized such that there was no film delamination as well as minimum TiC formation [28]. This layer was further subjected to PLA at an optimized energy density of 0.7±0.1 J/cm^2 necessary for the formation of Q-carbon [29]. PLD and PLA were carried out by utilizing state-of-the-art excimer lasers KrF (25 ns pulse duration) and ArF (20 ns pulse duration) having photon energies of 5 eV and 6.42 eV, respectively.

2.4. Characterization

An FEI Verios 460L SEM was employed for performing the HRSEM. The FIB Quanta SEM was employed to tilt the sample for better visualization of diamond growth and performing EBSD. The EBSD on diamond coating was performed by tilting the sample at 70°. The dynamic tilt correction feature was used to compensate for the scaling error due to tilt. The Kikuchi patterns obtained were compared with the database of Kikuchi bands of Fe, Cr, Ni, graphite, and Fe_3C. The XRD 2θ scans were performed using a Rigaku SmartLab X-ray diffractometer ($\lambda = 1.54$ A)in Bragg-Brentano in reflection geometry operating mode using a Cu Kα radiation source from a sealed tube operating at a voltage and current of 40 kV and 25 mA, respectively, and state of the art LENXEYE XE detector. A WITec confocal Raman microscope system (Alpha 300M – 532 nm laser source) with a grating size of 1800 I/mm was utilized to characterize the Raman-active vibrational modes in as-deposited and laser annealed samples. The Raman intensities were calibrated by making sure that the zero-loss peak was accurately observed at zero and Si peak at 520 cm^{-1}. The laser power of 30± 20 mW was utilized, and care was taken to prevent any unnecessary sample heating during the spectrum acquisition.

3. Results and discussions

3.1. Study of diamond growth on SS substrate utilizing surface pretreatment and Q-carbon interlayer

3.1.1. Utilization of surface scratching for enhanced diamond nucleation on SS 304/316

Fig. 1 depicts the ideal mechanism of diamond nucleation and growth on the SS substrate with and without surface scratch. In agreement with the observations on various substrates, scratching SS with a diamond scriber results in higher diamond nuclei spaced both closely and uniformly. However, on an unscratched SS substrate, the formation of diamond nuclei with a critical radius, r*, requires some incubation time, iron carbide/graphite interlayer also forms along with it on the substrate. The diamonds nucleate either in the interior or above this interlayer. The literature review indicates that this iron carbide/graphitic interlayer can be as large as 25 μm [30,31].

Fig. 2 illustrates the SEM images of selective diamond nucleation on the surface scratched region compared to the unscratched region on 304 and 316 SS substrates. The SS substrates were scratched with diamond scriber, which introduced surface roughness (Fig. 2(a-e)) . Fig. 2(a) depicts the preferential diamond nucleation and growth on surface scratched SS 304. Similar effect was observed in the case of SS 316 shown in Fig. 2(b). Fig. 2(c) is an image of SS 304 at high magnification close to the sample edge emphasizing the selective diamond nucleation on the surface scratch. Fig. 2(d) illustrates an image of CVD diamonds formed on diamond seeded SS and also surface scratched with a diamond scriber which as previously mentioned would introduce surface roughness. To investigate the improvement in the quality of microdiamonds formed on the surface scratch, the Raman spectra in the vicinity and inside the scratch region were acquired (Fig. 2f). The diamond peak was noted at 1332.8 cm^{-1}, sufficient to adduce the stress-free nature of the diamonds grown on these surface scratches [18]. It is interesting to note that the graphitic peak is absent even though Raman scattering occurs at higher efficiency (532 nm laser) for sp^2 bonded carbon (50–250 times) compared to sp^3 bonded carbon [32,33].

3.1.2. CVD diamond growth on silicon, sapphire in comparison with SS

The substrate-dependent growth of diamonds on different substrates (c-sapphire, silicon, and 304/316 austenitic SS) is shown in Fig. 3. The CVD diamond deposition conditions were the same for all of the substrates; all of the substrates were placed on the Mo plate and inserted at the same time in the CVD chamber. It is important to note that these substrates were not seeded with diamond nanoparticles prior to performing CVD. The number density of diamonds on the c-sapphire substrate is shown in Fig. 3(a) was found to be very low 10^6-$10^7/cm^2$. The number density of diamonds on the silicon substrate was comparatively higher than that on c-sapphire (Fig. 3 (b)). Diamonds grown on sapphire and silicon exhibited clear faceting with no traces of graphite. Fig. 3(c) shows the diamonds formed on 304 SS, small traces of graphite can be observed on the diamonds. The diamonds formed on 316 SS have been depicted in Fig. 3(d). Polycrystalline diamonds and higher graphitic content were found on SS 316 compared to SS 304. The large diamond nucleation and higher graphitic content on 316 SS

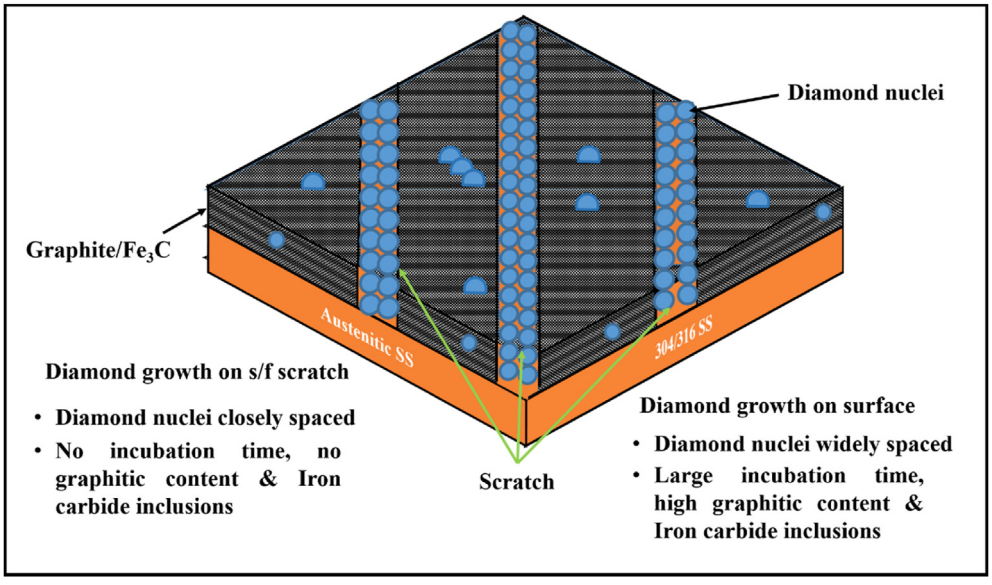

Fig. 1. Schematics of different diamond nucleation mechanisms on SS substrate on scratch, and unscratched region. (A colour version of this figure can be viewed online.)

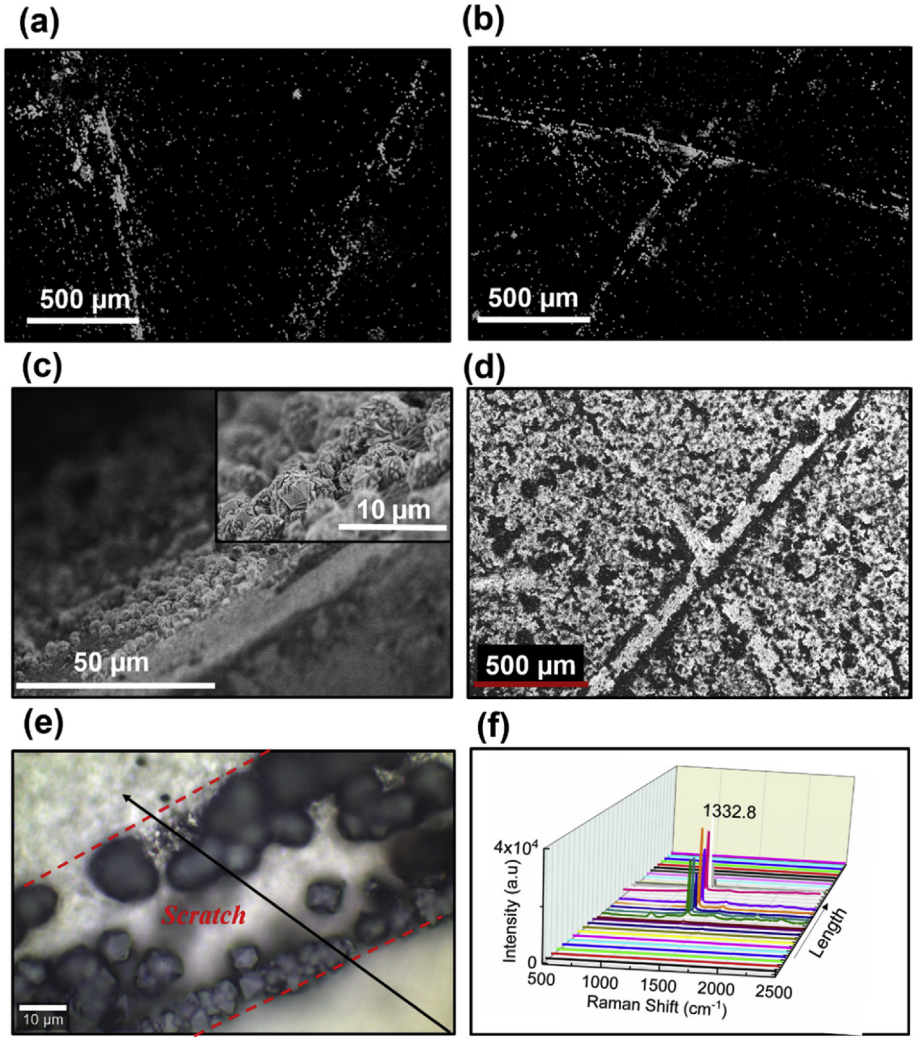

Fig. 2. SEM images of diamond growth on scratch: (a) SS 304; (b) SS 316; (c) SS 304 at low magnification close to substrate edge (inset) shows higher magnification image; (d) SS304 with diamond seeds; (e) Optical image on SS 304; (f) Raman spectra along the arrow shown in (e).

may be attributed to the presence of Mo, which is a carbide former, assisting in nucleation of both graphite and diamond. Previously, researchers have established that the substrate temperature in the range of 750–800 °C is optimum for austenitic SS in order to produce diamonds with minimum graphitic content and Fe_3C interlayer thickness [31]. Not to mention the fact that the minimum graphitic content is still pretty significant in the case of steels. The diamonds we synthesized on austenitic SS under the above-discussed conditions exhibited a polycrystalline nature along with a discernible amount of graphitic content.

3.1.3. Mechanism of enhanced nucleation due to surface roughening

The surface roughness increases the effective surface area, which may reduce the energy per unit area. This phenomenon, in turn, leads to the stabilization of smaller size diamond nuclei, i.e., the minimum critical radius (r*) for diamond nucleation is reduced. Another mechanism involved in the nucleation on rough surfaces during CVD is the nucleation by entrapment of diamond species, where metastable smaller nuclei are entrapped and grow. It is also possible that both these mechanisms may work concurrently and enhance diamond nucleation in scratched surfaces. It should be mentioned that similar enhancement is observed after roughening with PLA, which confirms the roughness as the primary cause of enhanced nucleation not any debris/impurity introduced by the diamond scriber [24].

For a metastable phase, such as diamond, the critical radius of nucleation (r*) under homogenous nucleation can be found by setting $\frac{dG_T}{dr} = 0$, where, ΔG_T is the total Gibbs free energy, ΔG^* Gibbs free energy per unit radius for transformation, and γ_s is the surface energy. The calculated value of r^* from equation (1) was ~1 nm.

$$r^* = \frac{2\gamma_s}{\Delta G^*} \tag{1}$$

Fig. 2(d) illustrates the SEM micrograph of the SS 304 substrate, which was polished with diamond paste and scratched with a diamond scriber. This sample showed uniform diamond nucleation throughout the sample, even in the non-scratched region, which illustrates the fact that the higher diamond nucleation is due to the presence of diamond seeds. However, the quality of diamonds formed on surface scratch was better than that on the surface seeded with diamond attributed to additional strains. Surface free energy of the substrate (σ_s) and film (σ_f) and the interfacial energy (σ_{sf}) determine the growth mode of the system [34].

$$\sigma_s < \sigma_f + \sigma_{sf} \tag{2}$$

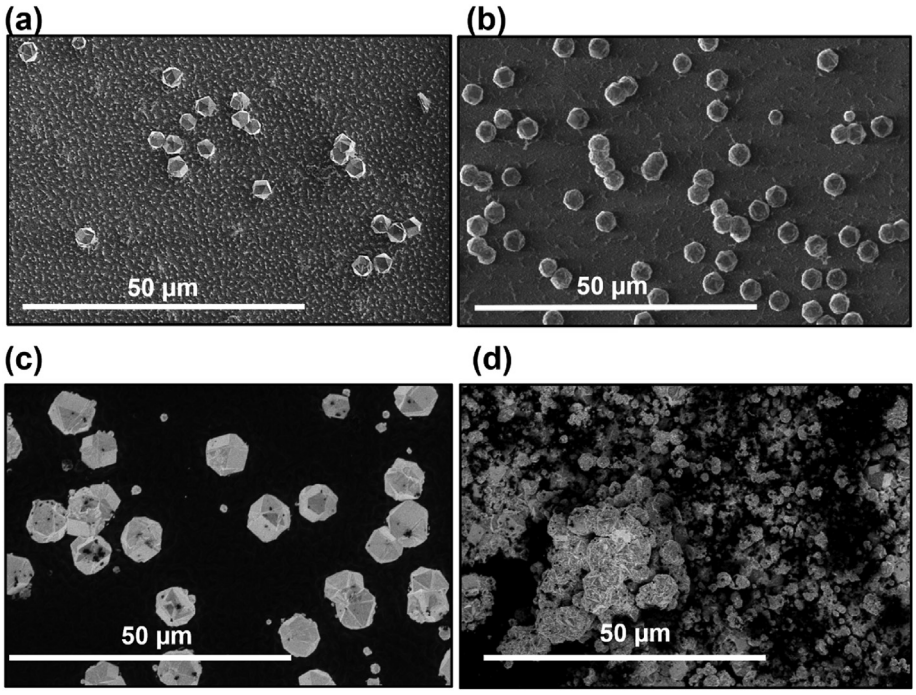

Fig. 3. HFCVD diamond growth on (a) c-sapphire; (b) Silicon; (c) SS 304; and (d) SS 316 after 6 h. (A colour version of this figure can be viewed online).

For 3D growth to transpire, the substrate and the film surface energy should be low, and the surface energy of the substrate film interface should be high. The substrate roughening promotes 3-D growth as it influences the surface energies. It decreases surface energy but increases interfacial energy. The roughened substrate is also thought to provide more nucleation sites.

3.1.4. CVD diamond on Q-carbon interlayer

To produce a superior quality diamond film on austenitic SS, our second approach was to utilize a Q-carbon interlayer. The advantage of the Q-carbon interlayer is its resemblance to the diamond crystal structure favoring the nucleation of the diamond. The Q-carbon structure consists of randomly packed diamond tetrahedra to generate higher number density of atoms than the diamond cubic crystal structure [15,20]. The unit cell of the diamond cubic structure has 8 atoms, whereas Q-carbon can accommodate as many as 12 atoms in the same unit cell dimensions [35].

Fig. 4(a) shows the glowing Q-carbon thin film through the cracked black α-carbon regions. The mechanism of cracking of α-carbon due to the formation of highly dense Q-carbon underneath it has been described elsewhere [36]. Etching of graphite (sp^2 rich) by hydrogen is a crucial step in obtaining high-quality CVD diamond. The literature on the mechanism of etching during CVD diamond growth suggests that the etching of the sp^1 and sp^2 bonded carbon is ten times faster than the etching of the sp^3 bonded carbon, which assists the growth of the sp^3 phase [37]. As has been previously reported in the literature [17,29,38,39], Q-carbon is sp^3 rich (~80% sp^3 and rest sp^2), its Raman spectrum is depicted in Fig. 4(c). We have observed that Q-carbon etches at the minimum rate, whereas as-deposited sp^2 rich DLC etches at a faster rate, which has been demonstrated in previous studies [18,19]. Fig. 4(d) shows the etching of the sp^2 rich DLC film. On the other hand, no such etching was observed on diamonds grown on the Q-carbon interlayer. Also, this figure qualitatively displays the less diamond nucleation on DLC interlayer compared to Q-carbon interlayer. In short, α-carbon is etched off, exposing Q-carbon, which provides nanodiamond seeds which further foster its growth during CVD to form microdiamonds. The microdiamonds formed on Q-carbon interlayer (Fig. 4(b)) contain fewer inclusions as compared to diamonds grown on bare SS substrate, as seen in Fig. 6(d). The diamond film grown on Q-carbon interlayer showed a sharp Raman signal at 1321 and at 1332 cm^{-1} (depicted in Fig. 5(c)), which is associated with nanodiamonds. The diamond peak at 1332 cm^{-1} (Fig. 5(d)) is ascribed to the presence of the T_{2g} vibrations [40], and this peak also signifies minimal residual stress in the grown diamond. The stress in diamond film on Q-carbon interlayer from Raman shift is given by Ref. [18]:

$$\Delta\nu\left[cm^{-1}\right] = \nu_s - \nu_o = -1.62\sigma[GPa] \quad (3)$$

The average Raman shift of diamond film grown on Q-carbon interlayer from equilibrium position of stress free diamond is 0.8 cm^{-1}. Using this data, a stress of 1.3 GPa has been obtained for the diamond film deposited on the Q-carbon interlayer. The obtained stress value in the diamond film grown on the Q-carbon interlayer is ~40% less than that grown on bare SS substrate..

The blue shift of the peak from 1332 to 1321 cm^{-1} is caused by the presence of nanodiamonds and is a result of phonon confinement effects [41]. Therefore, interestingly the diamond film synthesized on the Q-carbon interlayer is an amalgamation of both nanosized and micro-sized diamonds. The diamond surface shape is influential in determining its mechanical properties. The faceted diamonds exhibit poor toughness and are prone to chipping and fracture. However, the diamonds grown on the Q-carbon interlayer did not demonstrate any clear faceting and were found to be cauliflower (ballas) shaped as a result of copious nucleation. The ballas microstructure is formed by a grouping of many nanodiamonds, justifying the Raman peaks obtained at 1321 cm^{-1}. The ballas diamonds are obtained for higher carbon to hydrogen ratio (i.e., CH_4/H_2 ratio for enhanced nucleation. The higher nucleation can be envisaged to be coming from Q-carbon interlayer. It has been shown that the nanotwins in these nanodiamonds do not follow

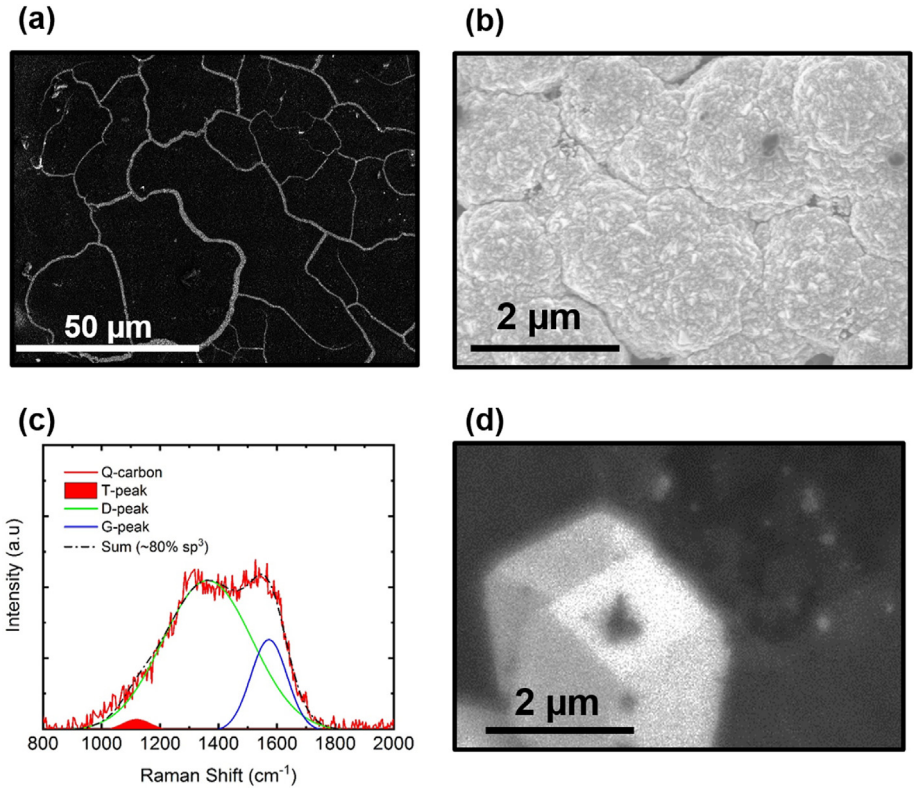

Fig. 4. (a) SEM micrograph of Q-carbon (white) below α-carbon on 316 SS substrates by PLA processing at 0.6 J/cm^2; (b) Continuous ballas type diamond film grown on Q-carbon interlayer after 3 h of HFCVD; (c) Q-carbon Raman spectrum; and (d) SEM image showing etching of DLC layer and less diamond nucleation compared to on Q-carbon interlayer after 3 h of HFCVD. (A colour version of this figure can be viewed online.)

the inverse Hall-Petch equation, i.e., the strengthening does not decrease below a definite twin size [42,43]. Twin boundaries are supposed to toughen the material by deflecting the cracks during crack initiation and propagation [44]. Twinning in diamond changes the crystal structure from face-centered cubic ABCABC stacking to hexagonal ABAB stacking. The twins, if present in alternating planes, can cause the formation of the hexagonal diamond phase, which has only three independent slip systems. Thus, reduction in slip systems is responsible for dislocation pile up and enhanced hardening. The extraordinary toughness and wear-resistance of ballas diamonds are attributed to the high amount of nanotwins, making them industrially relevant [45]. The diamond phase purity can be quantified by using the theory of Quality factor (Q) defined as [42]:

$$Q = \frac{sp^3}{sp^2} = \frac{I_{diamond}}{I_{diamond} + \frac{I_{a-carbon}}{233}} \quad (4)$$

where $I_{a\text{-carbon}}$ is the sum of Raman intensities of the observed non-diamond lines [46], the Raman spectra of diamonds obtained on scratch, Q-carbon interlayer, and bare SS substrate have been portrayed in Fig. 5. The quality factor of each was calculated to compare them for different conditions, $Q_1 > Q_2 > Q_3$ was noted. The subscripts 1, 2 and 3 correspond to microdiamond on scratch, Q-carbon interlayer, and bare SS substrate.

The XRD plots in Fig. 7 shows various important structural characteristics of diamond films deposited on the SS substrate with and without the presence of Q-carbon and DLC interlayer. Fig. 7(a) illustrates the XRD plot of the bare SS substrate. This plot was helpful in deciphering the peaks that did not originate from the substrate. The broad diffraction peak exhibited by Q-carbon (Fig. 5(b)) helped to validate its amorphous structure [29]. The sharp CVD diamond {111} peak was observed for diamond films synthesized using 3 h CVD on bare SS substrate (Fig. 7(c)) and also on SS with Q-carbon interlayer shown in Fig. 7(d). The XRD spectral acquisition was also carried out in the 2θ range of 70–100° illustrated in Fig. 7(e) and (f). The peaks observed at ~75° and 91° were identified to be diamond (220) and (311) peaks, respectively, which unambiguously confirmed the presence of diamond. Notably, the chromium carbide peak is found to be existent after CVD on as-received SS 316, while it is absent/very diffused on CVD coated SS 316 with Q-carbon interlayer present. As the chromium carbide is thought to be a brittle phase, the CVD coated SS 316 with the presence of a Q-carbon interlayer is expected to preserve toughness at the substrate-coating interface. By taking into consideration the Fe_3C intensity as a function of θ and variation of intensity of diamond $\left(\frac{I_{111}}{I_{220}}\right)$ as 2.83, the ratio of number density (N) $\left(\frac{N_{111}}{N_{220}}\right)$ for the diamond was found to be 0.53 for 6 h CVD for both 304 and 316 SS (Fig. 7 (e, f)).

The diamond thin film on Q-carbon interlayer can safely be assumed plane stress condition ($\sigma_{zz} = 0$; $\varepsilon_{zz} \neq 0$). The θ-2θ X-ray diffraction scan (Fig. 5(d)) was utilized to measure the strain (ε_{zz}) around (110) peak.

$$\sigma = 2\varepsilon_{xx}\mu(1+\nu)/(1-\nu) \quad (5)$$

where, ν is the Poisson's ratio = 0.2 $\varepsilon_{xx} = 1x10^{-3}$; $\mu = 455GPa$[35];

$$\sigma = 1365\varepsilon_{xx}\ GPa = 1.365\ \text{GPa}$$

Based on the above discussion, it can be presumed that Q-carbon can be used as a very effective interlayer to nucleate and

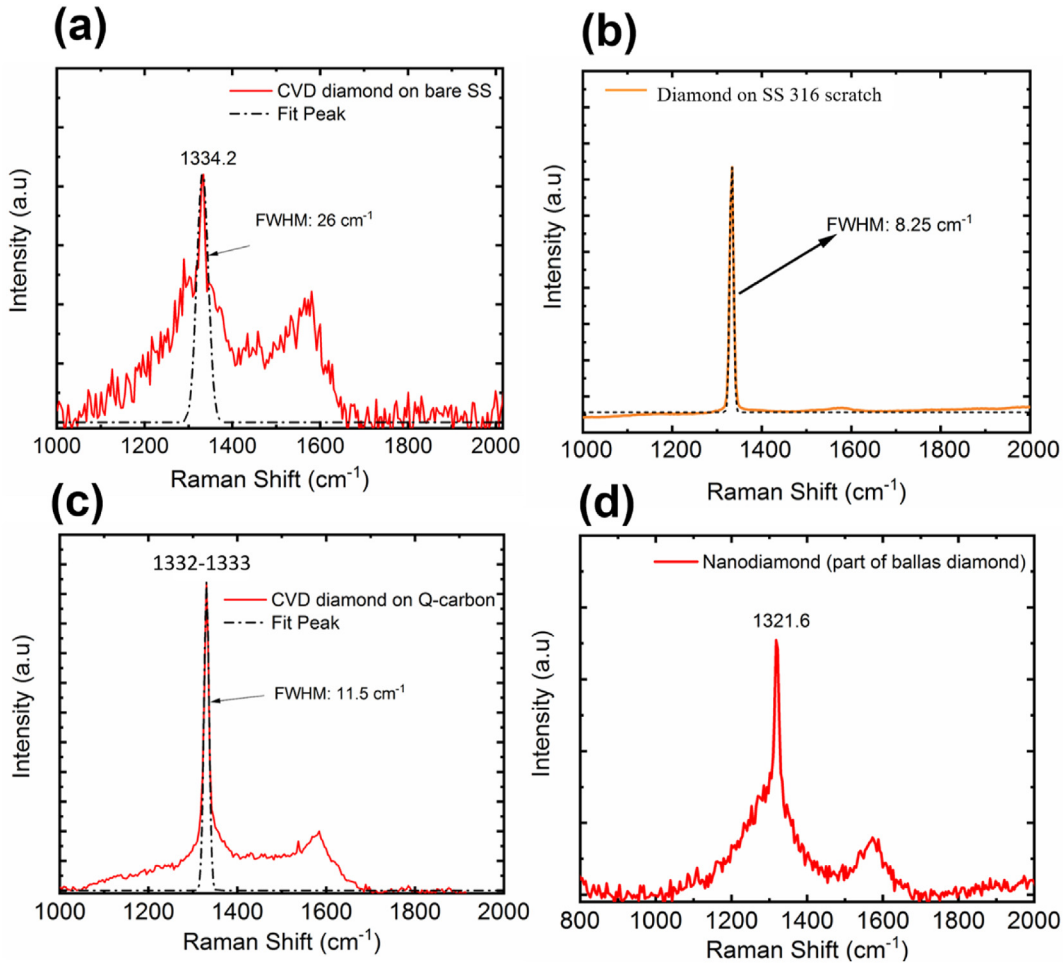

Fig. 5. Raman spectrum of (a) diamonds grown on bare SS 316 substrate; (b) diamonds grown on scratch; (c) microdiamonds grown on Q-carbon after CVD; and (d) nanodiamonds grown on Q-carbon seed layer. (A colour version of this figure can be viewed online.)

produce diamond coatings with higher hardness, toughness, and adhesion. We found that both scratching and Q-carbon interlayer is beneficial for obtaining high-quality CVD diamonds. However, scratching produces better quality diamonds compared to the Q-carbon interlayer FWHM of 8.25 cm^{-1} compared to 13 cm^{-1}. For some specific applications, a smooth and clean interface between diamond film and the substrate is essential. For very hard substrates, it is not possible to obtain reproducible surface scratches by using abrasives. Hence, the Q-carbon interlayer is ideal for those cases.

3.2. Diamonds formed on bare SS substrate (diamonds with Fe inclusions)

3.2.1. Formation of magnetic diamonds

The diamond nuclei entrenched in the graphitic interlayer may trap some iron particles diffusing from SS in them during its growth resulting in diamonds with iron inclusions, as shown previously [9]. The EBSD pattern taken on a continuous diamond film is displayed in Fig. 6 (a). Fig. 6 (c) demonstrates the presence of iron inclusions characterized using EBSD mapping (inset) on the diamonds grown on 304 SS. The characterized diamond showed <110> out of plane growth orientation, and the EBSD was taken along the <111> facet. Based on XRD and EBSD data, there were regions where diamonds grew along <110> orientation; however, in between these regions, diamonds with <111> out of plane orientation were also observed. The generation of iron carbide from iron is possible if iron from the substrate combines with amorphous carbon on the diamond surface. At 800 °C, the Fe cannot react with the diamond to form Fe_3C due to positive Gibbs free energy of the formation of iron carbide. In the temperature range of 400–800 °C, the diamond–Fe interaction is significantly lower [46]. The free energy for the formation of cementite becomes negative above ~963 °C, making the formation of cementite possible by extracting carbon present in the diamond and combining it with Fe [47].

$$Fe + 3C(Diamond) \rightarrow Fe_3C \quad \Delta G^o = 2.23\ \text{kJmol}^{-1}@800^\circ C \qquad (6)$$

In the proximity of 800 °C, the vapor pressure (P) of pure iron is 3.2×10^{-9} Torr [48]. The flux of iron particles can be calculated using equation (7):

$$\varphi_{Fe}\left(\frac{\#}{cm^2 s}\right) = 3.513 \times 10^{22}\frac{P\ (Torr)}{\sqrt{MT}} \qquad (7)$$

The SS ($M = 56$) substrates were square-shaped with a surface area of 1 cm^2 resulting in a value of $\varphi_{Fe} = 4.6 \times 10^{11}$ iron atoms/cm^2 s. This flux of Fe atoms ends up inside or above the diamond film. Based on SEM analysis, the average radius of the iron nanoparticle ~5 nm corresponding to a volume of 523.6 nm^3. In the case of bare unscratched SS substrate, the formation of diamond nuclei with critical radius r* requires some incubation time, along with the formation of diamond nuclei, iron carbide/graphite interlayer forms

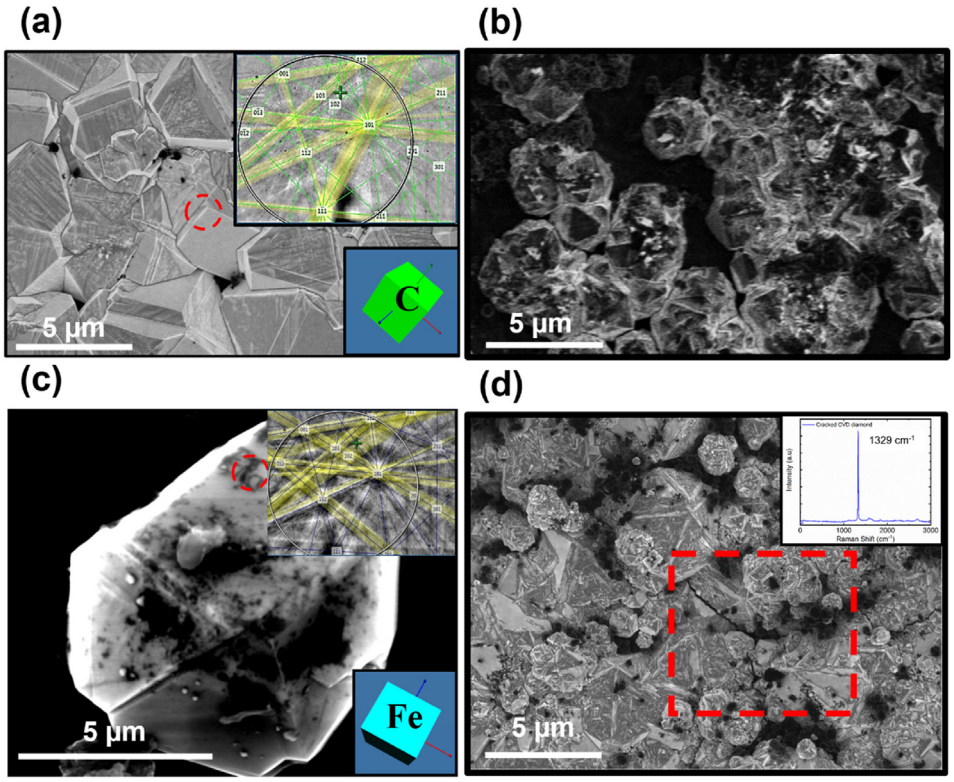

Fig. 6. SEM image of (a) continuous diamond film formed on SS 304 on scratch along with its EBSD from the dotted red-circled region showing <110> out of plane orientation of the diamond cubic crystal; (b) 3 h CVD growth on SS 316 showing the absence of a continuous diamond film; (c) Diamond with high graphitic content with iron inclusions as detected by EBSD; and (d) cracking in a continuous diamond film present on SS 316 with its Raman spectrum in the inset depicting the high stress present in the diamond film. (A colour version of this figure can be viewed online.)

on the substrate. The diamonds nucleate inside or over this interlayer (Fig. 1). During the diamond growth process, the iron atoms manage to evaporate from the substrate and diffuse into the diamonds. These iron atoms (~5×10^{16}/cm^2 for 6 h CVD) are sufficient to make these microdiamonds ferromagnetic, as shown in the past studies [9]. The atomic moment of Fe is 2.22 $\frac{\mu_B}{atom}$ [49–51]. One atom of Fe weights 9.27×10^{-23} g. So, the observed saturation magnetization of 0.3 emu corresponds to 1.35 mg of Fe. 1.35 mg of Fe corresponds to 1.45×10^{19} Fe atoms. Based on our experimental observations and calculations, $\varphi_{Fe} = 4.6 \times 10^{11}$ iron atoms/cm^2 s. For 6 h CVD, the total flux is 5×10^{16}/cm^2; the thickness of the diamond film is 6 μm, this results in 3×10^{19} Fe atoms. The flux of Fe atoms obtained in this study agrees pretty well with the flux of Fe atoms used to make diamond ferromagnetic by ion implantation [10]. These magnetic CVD diamonds may be mechanically converted to the powder form for applications such as MRI contrast agents, drug delivery to tumors, and SAW filters.

3.2.2. Cracking of the diamond film: calculation of film stress

In the case of SS 304 surface scratch after 6 h CVD growth, the number of diamond grains has increased sharply, and they coalesce to form an excellent continuous diamond film, which is not possible without scratching. For a diamond thin film with uniform coverage on scratch, a high density of five-fold twins was observed (Fig. 6(a)). The twin boundaries in the diamond are coherent with the absence of dislocations. High-resolution transmission electron microscopy investigations on twins in diamond have indicated that the angles between the {111} planes vary from 70o-74°. Interestingly, this substantial distortion is accommodated by elastic strains [52]. However, the rapid growth of interlayer phases such as iron carbide and chromium carbide results in the embedding of the diamonds within the porous interlayer observed in Fig. 6(d) on unscratched region of SS. It is evident that the diamonds formed on the unscratched surface, which nucleate on the interposing graphitic layers, have weak adhesion. The weak adhesion was further confirmed with a qualitative scotch tape test. Fundamental characteristic properties of thin-films depend on the strains present in them. At 25 °C, the CTE of austenitic SS is ~16 times that of the diamond [11]. The formed diamond film on austenitic SS 316 surface without the scratch was highly stressed, resulting in cracking (Fig. 6(d)). Cracking in the diamond film occurs when the diamond film is under tensile stress, which is evident from the Raman spectrum depicted in Fig. 6(d) inset. This Raman peak is shifted from its equilibrium stress-free position by 3.5 cm^{-1}. By using the above equation, a tensile stress of 2.1 GPa has been obtained in the diamond film. From the XRD data (Fig. 5(e and f)), the stress in the diamond film was calculated by using equation (5). We measured the strain (ε_{zz}) around (220) peak. We found an in-plane lattice strain of around 1.7×10^{-3}. The in-plane stress in the diamond film can be calculated using the value of obtained planar lattice strain and assuming $\varepsilon_{xx} = \varepsilon_{yy}$. The calculated stress in the diamond film is ~2.3 GPa, which matches well with the stress value measured from Raman analysis.

3.2.3. Surface features and morphology of diamonds observed on austenitic SS 304

The morphology of diamonds fabricated by CVD can be manipulated by varying the substrate temperature and CH_4/H_2

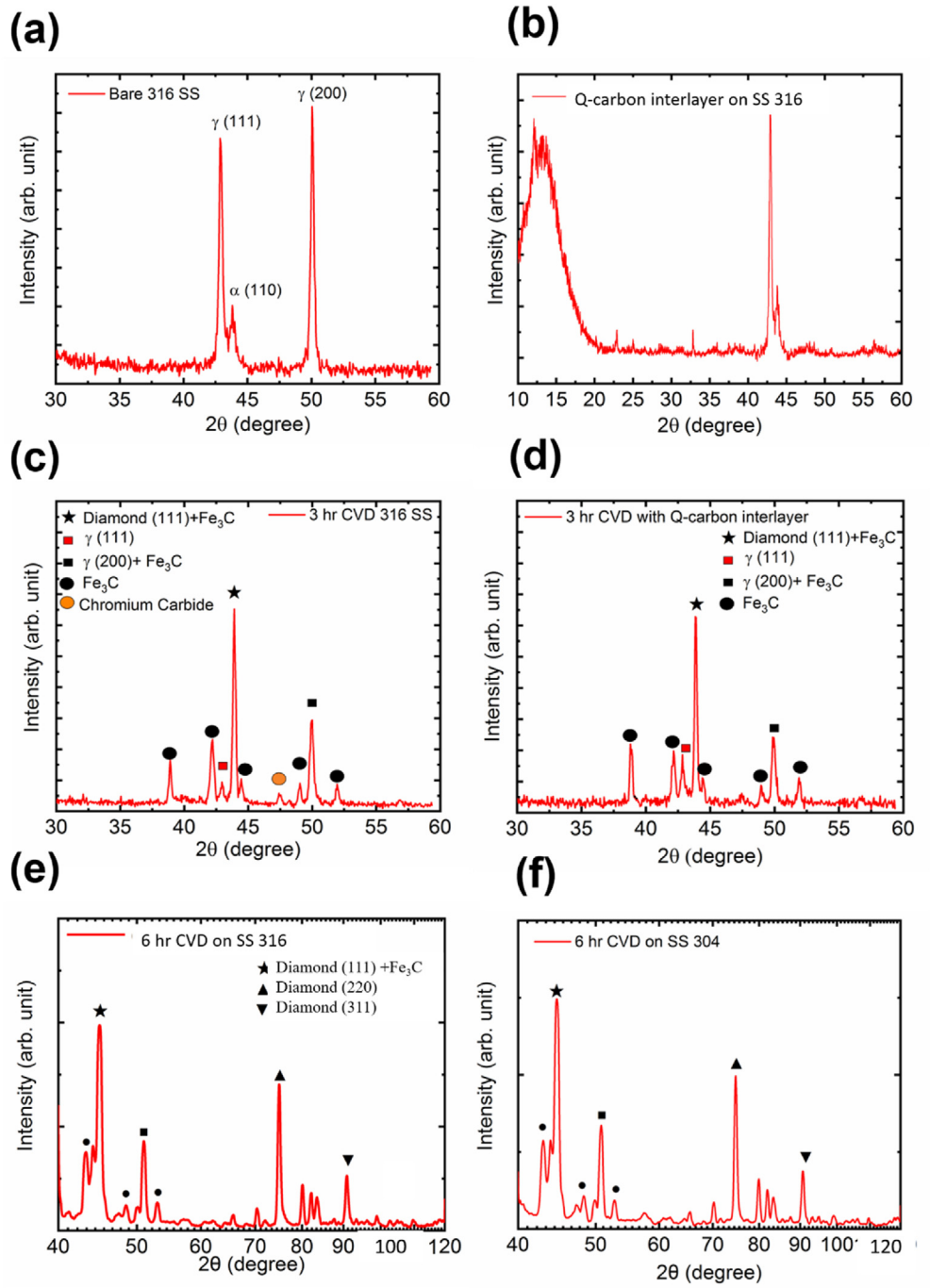

Fig. 7. XRD plots of (a) as-received 316 SS; (b) Q-carbon interlayer on 316 SS; (c) CVD on bare 316 SS; (d) CVD on 316 SS with the presence of Q-carbon interlayer; (e) 6 h CVD on bare 316 SS; and (f) 6 h CVD on bare 304 SS. (A colour version of this figure can be viewed online.)

ratio during deposition. The diamond shape is dictated by the growth rate in various directions. In general, for diamonds synthesized by CVD, if we compare the growth rate along <111>, <100> and <110>; <111> has the slowest growth velocity (v_{111}), whereas <110> has relatively moderate growth velocity (v_{110}), and <100> has the fastest growth velocity (v_{100}) [53].

$$\beta = \sqrt{3}\ \frac{v_{100}}{v_{111}} \tag{8}$$

The higher the value of β, the higher the fraction of the {111} faces dominating the shape of the diamond.

As shown in Fig. 8, diverse diamond morphologies were achieved on the SS 304 substrate after 3 h HFCVD deposition. The different shapes can be explained by equation (8) [6]. Diamond (cuboctahedron with <100> added faces) morphology shown in Fig. 8 (a) is obtained when the value of β varies in the range of 1.5–2. This morphology was observed at the sample edges. From the literature, this value of β corresponds to the methane concentration of 0.5–1% lower than the required value of 2%, which is possible at the very edge of the sample. Diamonds in the central region of the substrate showed morphology corresponding to the methane concentration of 2–2.5% (Fig. 8(b)).

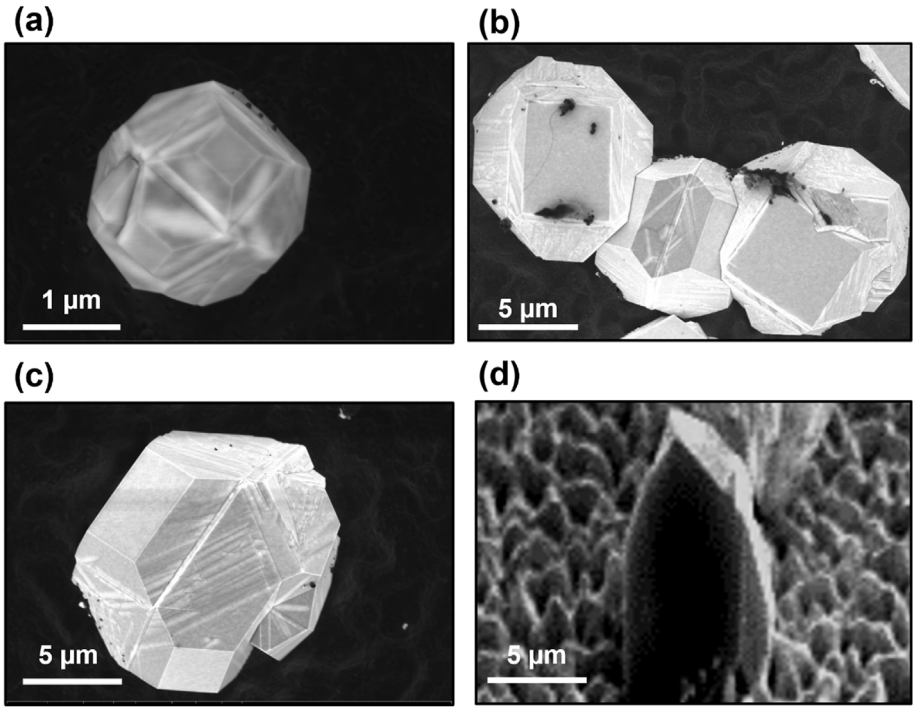

Fig. 8. SEM images of different diamond morphologies found on SS 304 at (a) $\beta \sim 1.5 - 2$; (b)$\beta \sim 2.5 - 3$; (c) diamond exhibiting many twins; and (d) tilted SEM highlighting the <110> growth of diamonds.

4. Conclusions

In conclusion, to synthesize diamonds without any inclusions/graphitic content, we investigated the role of Q-carbon interlayer and surface scratching pre-treatment on austenitic SS. Both approaches were effective in producing a higher density of diamonds with minimal stress and graphitic content. In the case of Q-carbon, there are pre-existing nucleation sites that foster diamond growth. Whereas substrate roughening affects the surface and interfacial energy, assisting in both 3D diamond growth and generation of more nucleation sites. Notably, diamonds synthesized on Q-carbon interlayer are expected to be stronger and tougher compared to usually faceted diamonds as they were ballas type (indicating higher twin concentration). The utilization of a Q-carbon interlayer to grow high-quality diamond coatings is industrially scalable. Furthermore, CVD diamonds synthesized on bare austenitic SS 304/316 substrates show presence of Fe inclusions characterized by using EBSD. The Fe atoms evaporate from the substrate into the diamond as a result of high substrate temperature (>750 °C). From the free energy estimations, we establish that the formation of Fe_3C is more favorable than Fe at substrate temperatures over 960 °C. The possibility for the formation of Fe_3C inclusions opens up new prospects for imparting more robust ferromagnetism in diamonds. This study provides a general roadway for tailoring the properties of CVD diamonds on austenitic stainless-steel substrate handy for uses in MRI, drug delivery to tumors, SAW filters, and magnetic semiconductors for electronic applications.

CRediT authorship contribution statement

Pratik Joshi: Formal analysis, Writing - original draft, Writing - original draft, conducted the materials synthesis, Raman spectroscopy, HRSEM imaging, X-ray diffraction, wrote the manuscript with the inputs from all co-authors. **Ariful Haque:** Formal analysis, HFCVD. **Siddharth Gupta:** Formal analysis, EBSD. **Roger J. Narayan:** Conceptualization, Funding acquisition, conceived the project and funding. **Jagdish Narayan:** Conceptualization, Funding acquisition, conceived the project and funding.

Declaration of competing interest

The authors declare that they have no known competing financial interests or personal relationships that could have appeared to influence the work reported in this paper.

Acknowledgment

We are grateful to Fan Family Foundation Distinguished Chair Endowment for J. Narayan. This research work was jointly performed under the National Science Foundation (Award Number DMR- 2016256), Project Award Agreement from the National Institute for Innovation in Manufacturing Biopharmaceuticals (NIIMBL), and financial assistance award 70NANB17H002 from the US Department of Commerce, National Institute of Standards and Technology. The characterization part (SEM) was conducted at the Analytical Instrumentation Facility (AIF) at North Carolina State University, which is supported by the State of North Carolina.

Appendix A. Supplementary data

Supplementary data to this article can be found online at https://doi.org/10.1016/j.carbon.2020.09.064.

References

[1] Material properties of diamond (n.d.), https://www.cs.mcgill.ca/~rwest/wikispeedia/wpcd/wp/m/Material_properties_of_diamond.htm (accessed April 20, 2020).
[2] S. Castelletto, L. Rosa, J. Blackledge, M.Z. Al Abri, A. Boretti, Advances in diamond nanofabrication for ultrasensitive devices, Microsyst. Nanoeng. 3 (2017) 1–16, https://doi.org/10.1038/micronano.2017.61.
[3] X. Chen, W. Zhang, Diamond nanostructures for drug delivery, bioimaging, and biosensing, Chem. Soc. Rev. 46 (2017) 734–760, https://doi.org/10.1039/c6cs00109b.

[4] A. Krueger, Diamond nanoparticles: jewels for chemistry and physics, adv, Materials 20 (2008) 2445–2449, https://doi.org/10.1002/adma.200701856.

[5] H.G. Zanin, A.C. Mpeterlevitz, R.F. Teófilo, H.J. Ceragioli, V. Baranauskas, Synthesis and characterization of magnetic nanocrystalline diamond films, Ferroelectrics (2012) 96–100, https://doi.org/10.1080/10584587.2012.731340. Taylor & Francis Group.

[6] M. Piazzi, M. Morana, M. Coïsson, F. Marone, M. Campione, L. Bindi, A.P. Jones, E. Ferrara, M. Alvaro, Multi-analytical characterization of Fe-rich magnetic inclusions in diamonds, Diam. Relat. Mater. 98 (2019), https://doi.org/10.1016/j.diamond.2019.107489.

[7] F.V. Kaminsky, R. Wirth, Iron carbide inclusions in lower-mantle diamond from juina, Brazil, Can. Mineral. 49 (2011) 555–572, https://doi.org/10.3749/canmin.49.2.555.

[8] H.K.D.H. Bhadeshia, Cementite FULL CRITICAL REVIEW cementite. https://doi.org/10.1080/09506608.2018.1560984, 2019.

[9] H. Zanin, A.C. Peterlevitz, H.J. Ceragioli, A.A. Rodrigues, W.D. Belangero, V. Baranauskas, Magnetic and cytotoxic properties of hot-filament chemical vapour deposited diamond, Mater. Sci. Eng. C 32 (2012) 2340–2343, https://doi.org/10.1016/j.msec.2012.07.005.

[10] B.R. Lin, C.H. Chen, S. Kunuku, T.Y. Chen, T.Y. Hsiao, H. Niu, C.P. Lee, Fe doped magnetic nanodiamonds made by ion implantation as contrast agent for MRI, Sci. Rep. 8 (2018) 7058, https://doi.org/10.1038/s41598-018-25380-1.

[11] X. Chen, J. Narayan, Effect of the chemical nature of transition-metal substrates on chemical-vapor deposition of diamond, J. Appl. Phys. 74 (1993) 4168–4173, https://doi.org/10.1063/1.354420.

[12] S. Gupta, R. Sachan, A. Bhaumik, J. Narayan, Enhanced mechanical properties of Q-carbon nanocomposites by nanosecond pulsed laser annealing, Nanotechnology 29 (2018), https://doi.org/10.1088/1361-6528/aadd75, 45LT02.

[13] Coefficients of Linear Thermal Expansion (n.d.), https://www.engineeringtoolbox.com/linear-expansion-coefficients-d_95.html (accessed May 28, 2020).

[14] D. Damm, A. Contin, F. Barbieri, V. Trava-Airoldi, D. Barquete, E. Corat, Interlayers applied to CVD diamond deposition on steel substrate: a review,, Coatings 7 (2017) 141, https://doi.org/10.3390/coatings7090141.

[15] A. Haque, J. Narayan, Electron field emission from Q-carbon, Diam. Relat. Mater. 86 (2018) 71–78, https://doi.org/10.1016/j.diamond.2018.04.008.

[16] S. Gupta, J. Narayan, Selective liquid-phase regrowth of reduced graphene oxide, nanodiamond, and nanoscale Q-carbon by pulsed laser annealing for radiofrequency devices, ACS Appl. Nano Mater. 3 (2020) 5178–5188, https://doi.org/10.1021/acsanm.0c00609.

[17] P. Joshi, S. Gupta, A. Haque, J. Narayan, Fabrication of ultrahard Q-carbon nanocoatings on AISI 304 and 316 stainless steels and subsequent formation of high-quality diamond films, Diam. Relat. Mater. 104 (2020) 107742, https://doi.org/10.1016/j.diamond.2020.107742.

[18] A. Haque, P. Pant, J. Narayan, Large-area diamond thin film on Q-carbon coated crystalline sapphire by HFCVD, J. Cryst. Growth 504 (2018) 17–25, https://doi.org/10.1016/j.jcrysgro.2018.09.036.

[19] A. Haque, J. Narayan, Conversion of h-BN into c-BN for tuning optoelectronic properties, Mater. Adv 1 (2020) 830–836. https://doi.org/10.1039/D0MA00008F.

[20] A. Haque, J. Narayan, Stability of electron field emission in Q-carbon, MRS Commun. 8 (2018) 1343–1351, https://doi.org/10.1557/mrc.2018.172.

[21] S. Gupta, R. Sachan, A. Bhaumik, P. Pant, J. Narayan, Undercooling driven growth of Q-carbon, diamond, and graphite, MRS Commun. 8 (2018) 533–540, https://doi.org/10.1557/mrc.2018.76.

[22] A. Haque, S. Gupta, J. Narayan, Characteristics of diamond deposition on Al2O3, diamond-like carbon and Q-carbon, ACS Appl. Electron. Mater. 2 (5) (2020), https://doi.org/10.1021/acsaelm.0c00106.

[23] R.K. Singh, D.R. Gilbert, J. Fitz-Gerald, S. Harkness, D.G. Lee, Engineered interfaces for adherent diamond coatings on large thermal-expansion coefficient mismatched substrates, Science 272 (1996) 396–398, https://doi.org/10.1126/science.272.5260.396 (80-.).

[24] J. Narayan, X. Chen, Laser patterning of diamond films, J. Appl. Phys. 71 (1992) 3795–3801, https://doi.org/10.1063/1.350892.

[25] A. Bhaumik, S. Nori, R. Sachan, S. Gupta, D. Kumar, A.K. Majumdar, J. Narayan, Room-temperature ferromagnetism and extraordinary Hall effect in nanostructured Q-carbon: implications for potential spintronic devices. https://doi.org/10.1021/ACSANM.7B00253, 2018.

[26] S. Gupta, J. Narayan, Direct conversion of Teflon into nanodiamond films, Mater. Res. Lett. 8 (2020) 408–416, https://doi.org/10.1080/21663831.2020.1778111.

[27] B.V. Spitsyn, L.L. Bouilov, B.V. Derjaguin, Vapor growth of diamond on diamond and other surfaces, J. Cryst. Growth 52 (1981) 219–226. https://doi.org/10.1016/0022-0248(81)90197-4.

[28] Y. Zhou, L. Li, W. Shao, Z. Chen, S. Wang, X. Xing, Q. Yang, Mechanical and tribological behaviors of Ti-DLC films deposited on 304 stainless steel: exploration with Ti doping from micro to macro, Diam. Relat. Mater. 107 (2020), https://doi.org/10.1016/j.diamond.2020.107870.

[29] R. Sachan, S. Gupta, J. Narayan, Nonequilibrium structural evolution of Q-carbon and interfaces, ACS, Appl. Mater. Interfaces 12 (2020) 1330–1338, https://doi.org/10.1021/acsami.9b17428.

[30] J.G. Buijnsters, P. Shankar, J.J. Ter Meulen, Direct deposition of polycrystalline diamond onto steel substrates, Surf. Coating. Technol. 201 (2007) 8955–8960, https://doi.org/10.1016/j.surfcoat.2007.04.012.

[31] J.G. Buijnsters, P. Shankar, W.J.P. Van Enckevort, J.J. Schermer, J.J. Ter Meulen, The applicability of ultra thin silicon films as interlayers for CVD diamond deposition on steels,, Phys. Status Solidi Appl. Res. 195 (2003) 383–395, https://doi.org/10.1002/pssa.200305947.

[32] N. Wada, P.J. Gaczi, S.A. Solin, "Diamond-like" 3-fold coordinated amorphous carbon, J. Non-Cryst. Solids 35–36 (1980) 543–548, https://doi.org/10.1016/0022-3093(80) 90651–1.

[33] S.R. Sails, D.J Gardiner, M. Bowden, J. Savage, D. Rodway, Monitoring the quality of diamond films using Raman spectra excited at 514.5 nm and 633 nm, Diam. Relat. Mater 5 (1996) 589–591. https://doi.org/10.1016/0925-9635(96)90031-x.

[34] J. Narayan, Recent progress in thin film epitaxy across the misfit scale (2011 Acta Gold Medal Paper), Acta Mater. 61 (2013) 2703–2724, https://doi.org/10.1016/j.actamat.2012.09.070.

[35] J. Narayan, A. Bhaumik, S. Gupta, A. Haque, R. Sachan, Progress in Q-Carbon and Related Materials with Extraordinary Properties BRIEF OVERVIEW Progress in Q-Carbon and Related Materials with Extraordinary Properties vol. 6, 2018, pp. 353–364, https://doi.org/10.1080/21663831.2018.1458753.

[36] S. Gupta, R. Sachan, J. Narayan, Scale-up of Q-carbon and nanodiamonds by pulsed laser annealing, Diam. Relat. Mater. 99 (2019), https://doi.org/10.1016/j.diamond.2019.107531.

[37] H. Sumiya, N. Toda, S. Satoh, Growth rate of high-quality large diamond crystals, J. Cryst. Growth 237–239 (2002) 1281–1285, https://doi.org/10.1016/S0022-0248(01) 02145–5.

[38] J. Narayan, A. Bhaumik, Novel phase of carbon, ferromagnetism, and conversion into diamond, J. Appl. Phys. 118 (2015), https://doi.org/10.1063/1.4936595.

[39] H. Yoshinaka, S. Inubushi, T. Wakita, T. Yokoya, Y. Muraoka, Formation of Q-carbon by adjusting sp3 content in diamond-like carbon films and laser energy density of pulsed laser annealing, Carbon N. Y. 167 (2020) 504–511, https://doi.org/10.1016/j.carbon.2020.06.025.

[40] R.S. Krishnan, Raman spectrum of diamond [2], Nature 155 (1945) 171, https://doi.org/10.1038/155171a0.

[41] S. Prawer, R.J. Nemanich, Raman spectroscopy of diamond and doped diamond, Philos. Trans. A. Math. Phys. Eng. Sci 362 (2004) 2537–2565, https://doi.org/10.1098/rsta.2004.1451.

[42] H. Conrad, J. Narayan, On the grain size softening in nanocrystalline materials, Scripta Mater. 42 (2000) 1025–1030, https://doi.org/10.1016/S1359-6462(00)00320-1.

[43] Q. Huang, D. Yu, B. Xu, W. Hu, Y. Ma, Y. Wang, Z. Zhao, B. Wen, J. He, Z. Liu, Y. Tian, Nanotwinned diamond with unprecedented hardness and stability, Nature 510 (2014) 250–253, https://doi.org/10.1038/nature13381.

[44] Z.W. Shan, L. Lu, A.M. Minor, E.A. Stach, S.X. Mao, The effect of twin plane spacing on the deformation of copper containing a high density of growth twins,, JOM (J. Occup. Med.) 60 (2008) 71–74, https://doi.org/10.1007/s11837-008-0122-z.

[45] D. Das, R.N. Singh, A review of nucleation, growth and low temperature synthesis of diamond thin films, Int. Mater. Rev 52 (2007) 29–64, https://doi.org/10.1179/174328007X160245.

[46] S. Zenkin, A. Gaydaychuk, V. Okhotnikov, S. Linnik, CVD diamond interaction with Fe at elevated temperatures, Materials 10 (2018), https://doi.org/10.3390/ma11122505.

[47] S.R. Shatynski, The Thermochemistry of Transition Metal Carbides, 1979.

[48] Vapor Pressure Calculator [IAP/Tu Wien] (n.d.), https://www.iap.tuwien.ac.at/www/surface/vapor_pressure (accessed March 17, 2020).

[49] S. Bï, C 1 Reduced Dimensions I: Magnetic Moment and Magnetic Structure, (n.d).

[50] Magnetic Generator (You can change emu–> Bohr magneton) (n.d.), http://www.az.appi.keio.ac.jp/satohlab/mg.html (accessed September 1, 2020).

[51] Magnetic Units (n.d.), http://www.ieeemagnetics.org/index.php?option=com_content&view=article&id=118&Itemid=107 (accessed September 1, 2020).

[52] J. Narayan, A.R. Srivatsa, K.V. Ravi, Mechanism of formation of ⟨110⟩ oriented fivefold microcrystallites in diamond films, Appl. Phys. Lett. 54 (1989) 1659–1661, https://doi.org/10.1063/1.101297.

[53] Handbook of Industrial Diamonds and Diamond Films - Google Books (n.d.), https://books.google.com/books?id=73uCDwAAQBAJ&pg=PP33&lpg=PP33&dq=%3C111%3E+is+the+slowest+growth+direction.+%3C110%3E+is+the+fastest+growth+direction+diamond.&source=bl&ots=70cbss1gyP&sig=ACfU3U1ts3bdniXWo7k7aMT_bqFaOZf_mQ&hl=en&sa=X&ved=2ahUKEwjnhrKn5a7oAhUMmHIEHa49ATMQ6AEwAHoECAoQAQ#v=onepage&q&f=false (accessed March 22, 2020).